Food Analytical Methods (2020) 13:420–432
https://doi.org/10.1007/s12161-019-01652-y

Detection of Inosine Monophosphate (IMP) in Meat Using Double-Enzyme Sensor

Guangxian Wang[1] · Jianfei Sun[1] · Yao Yao[1] · Xingshuang An[1] · Hui Zhang[1] · Guanglei Chu[1] · Shui Jiang[2] · Yemin Guo[1] · Xia Sun[1] · Yuan Liu[2]

Received: 19 July 2019 / Accepted: 22 September 2019 / Published online: 12 November 2019

Abstract

Inosine monophosphate (IMP) was considered to be an important component of meat flavor and an important indicator for evaluating the quality of meat products. This paper developed a novel dual-enzyme biosensor for the quantitative detection of inosinic acid to assess meat quality. Using the conductivity of MXene materials and the ability of Au@Pt nanoflowers to catalyze the oxidation of H_2O_2, a dual-enzyme biosensor was assembled and prepared for sensitive and rapid detection of IMP. The MXene-Ti_3C_2Tx material had 2D nanostructure similar to that of graphene, as well as metal conductivity and good biocompatibility. MXene was used as a carrier for 5′-nucleotidase and xanthine oxidase, with good biological environment and stable microenvironment. Bimetallic nanoflowers with a core-shell structure had better ability to catalyze H_2O_2 than the single metal. The double-enzyme hydrolyzed IMP to produce the H_2O_2. The Au@Pt nanoflowers of the sensor can catalyze the decomposition of H_2O_2, which causes electron transfer to produce current change. Therefore, the content of IMP is indirectly obtained by monitoring the current change. The results showed that the linear range of the double-enzyme biosensor was 0.04~17 g L^{-1}, the correlation coefficient was 0.9964, and the detection limit was 2.73 ng mL^{-1}. The biosensor had great reproducibility and stability. Compared with high-performance liquid chromatography, biosensors could quickly and accurately detect the content of inosine monophosphate in meat, and provided a better method to detect the quality index of meat products.

Keywords Transition metal carbide · Au@Pt nanoflowers · Enzyme biosensor · Inosine monophosphate

Highlights

1. Developed a new dual-enzyme biosensing system for the determination of IMP.
2. Design and synthesis of a novel Mxene(Ti_3C_2Tx)-Pt@Au nanoflower composite film with conductivity and biocompatibility.
3. The results showed that the enzyme biosensor had a good linear relationship in the range of from 0.04 to 17 g L^{-1}, the correlation coefficient was 0.9964, and the detection limit was 2.73 ng mL^{-1}.
4. A novel enzyme biosensor was developed to assess meat quality and freshness.

Electronic supplementary material The online version of this article (https://doi.org/10.1007/s12161-019-01652-y) contains supplementary material, which is available to authorized users.

✉ Yemin Guo
gym@sdut.edu.cn

Guangxian Wang
15288930360@163.com

[1] School of Agricultural Engineering and Food Science, Shandong University of Technology, No. 12 Zhangzhou Road, Zibo 255049, Shandong Province, China

[2] Department of Food Science and Technology, School of Agriculture and Biology, Shanghai Jiao Tong University, Shanghai 200240, China

Introduction

The meat quality is closely related to the components of the flavor substances such as inosinic acid, intramuscular fat, and free fatty acid, and the intensive taste of inosinic acid is the strongest (Zhang et al. 2019a, b). Inosinic acid (IMP), a hypoxanthine nucleotide, has an important influence on the water holding capacity, physical properties, and sensory properties of meat. It is one of the important umami substances in animal tissues and is closely related to the umami taste of meat products (Ngapo and Vachon 2016). IMP increases the umami taste of foods by 40 times stronger than that of sodium glutamate. The formation of IMP in the meat is accompanied by the decomposition of ATP in the muscle; the inosine acid continuously increased and then is decomposed by the action of phospholipase and nucleoside hydrolase to produce inosine and hypoxanthine (Ramalingam et al. 2019). The accumulation of hypoxanthine nucleotides and other decomposition products in the meat can make the umami rich, and the heating of IMP in water or fat can produce a distinct umami taste (Clausena et al. 2018). At present, IMP is an important indicator for meat quality assessment. The determination of IMP content in muscle tissue has been widely used in the quality assessment of various animal meat products. It has been recognized internationally as an important indicator for detecting meat umami taste. Conventionally, IMP is detected by thin-layer chromatography, high-pressure electrophoresis and ultraviolet spectrophotometry, and high-performance liquid chromatography. However, these methods require complicated processes and are low in sensitivity, time consuming, and costly. Therefore, there is an urgent need to develop a simple, rapid, and sensitive method for determining inosine.

With the increasing interest in low-dimensional nanomaterials, two-dimensional (2D) transition metal carbide or nitride has attracted more and more attention because of its unique form (Shukla et al. 2019; Guo et al. 2019; Li et al. 2017). MXene-$Ti_3C_2T_X$ is a new type of two-dimensional nanomaterial that is similar to graphene. Due to its striking physical and chemical properties, such as high specific surface area, high conductivity, high stability, and good dispersion in water, it has been widely used in electrochemical energy storage, catalysis, sensing, electromagnetic shielding, membrane separation technology, and so on (Tran et al. 2018; Wu et al. 2019; Li et al. 2018a, b, c).

MXene material is produced by etching the sp element layer from the corresponding three-dimensional (3D) MAX phase that is ternary metal carbide, nitride, and carbon nitride (Feng et al. 2017). Ti_3AlC_2 is one of over 70 ternary carbides and nitride ($M_{n+1}AX_n$). MXene-$Ti_3C_2T_X$ can be obtained by stripping Al using hydrofluoric acid. Because of the unsaturated surface with unpaired electrons (Li et al. 2015), it is easy to use various functional groups (such as –O, –OH, or –F groups) to seal the MXene-$Ti_3C_2T_X$ surface by etching process without changing the conductivity of the metal (Zhang et al. 2019a, b; Xu et al. 2018).

So far, MXene nanoparticles have been used in catalysis, sensing, and biosensors, as well as the adsorption of a large number of chemical substances (Lorencova et al. 2017). For example, glucose biosensor was developed by implanting nafion-AuNP-MXene nanocomposite onto a glassy carbon electrode (GCE). In the development of the biosensor matrix, MXene ($Ti_3C_2T_X$) shows high conductivity and improves electron transfer between the active redox center and the electrode interface of GOx. The sensing performance of the biosensor is greatly improved by Au nanoparticles, which reduces the over-potential of detecting hydrogen peroxide (H_2O_2), and H_2O_2 is a by-product produced during glucose oxidation (Lorencova et al. 2018). Recent studies have showed that the original form of MXene based on $Ti_3C_2T_X$ or combined with TiO_2 nanoparticles constructs a hemoglobin-based medium-free biosensor for detecting $NaNO_2$ (LOD = 120 nM) (Su et al. 2018; Chekem et al. 2019); the nanolayer has great biocompatibility and can achieve lower detection limits (Wang et al. 2015). Recently, the construction of the nanolayer has good biocompatibility and can achieve a low detection limit. In addition to biomolecule biosensors, MXene materials have good application prospects in environmental and agricultural fields. For example, MXene biosensors are used in pesticide detection. An acetylcholinesterase biosensor based on amperometric method is used for the detection of organophosphorus pesticides (Zhou et al. 2017). The enzyme is immobilized on MXene nanosheets, and can achieve rapid and specific detection of malathion pesticides. The developed sensor has high stability, high reproducibility, low detection limit, and excellent anti-interference ability for malathion oxidation detection; it provides a new platform for food safety monitoring. MXene materials have applicability in environmental and agricultural safety.

Au@Pt nanoflowers are synthesized on $Ti_3C_2T_X$ by reduction method. By using the ultra-high conductivity of $Ti_3C_2T_X$ material and the large specific surface area of the accordion structure, nanoparticles can obtain better catalytic effect, and the constructed Au@Pt nanoflowers have core-shell bimetallic open structures and abundant active sites. On the surface of the bimetallic catalyst, the Au particles are positively charged. The addition of a negatively charged second active metal (such as Pt) to the Au catalyst increases the negative charge region of the entire catalyst surface, facilitating the hydrogen peroxide decomposition reaction. The interaction with the electrons shows better catalytic activity with their single metal counterparts. 5′-nucleotidase and xanthine oxidase have good electrocatalytic activity for IMP, and the catalytic oxidation peroxidation of Au@Pt nanoflowers is monitored at the biosensor by using the by-product hydrogen peroxide produced in the two-step catalytic process. The current signal of

hydrogen is used as the detection target to achieve the purpose of qualitative and quantitative detection of IMP. The use of double-enzyme two-step catalysis has great advantages due to the good properties of biosensor, such as good specificity, low detection limit, and more obvious signals. MXene-$Ti_3C_2T_X$ with graphene structure has proven to be a robust electrochemical sensing platform for enzyme-based biosensors and has broad application prospects in biomedical monitoring and environmental analysis. Therefore, in this paper, MXene material loaded with Au@Pt nanoflowers is applied as sensing platform for the specific detection of IMP.

Experiment

Materials

5′-Nucleotidase, IMP, chloroplatinic acid, H_2PtCl_6, $HAuCl_4{\cdot}3H_2O$ (99.9%), and xanthine oxidase were obtained from Sigma-Aldrich (USA). Hydrogen peroxide, uric acid, acetic acid, and bovine serum albumin (BSA) were bought from Macklin (China). Phosphate buffer solution (PBS) was prepared by mixing stock standards of Na_2HPO_4 and NaH_2PO_4; all other chemicals were of analytical grade and used as received, all prepared in ultrapure deionized water (DW).

Instruments and Methods

XRD images of MXene solution were obtained by X-ray diffractometer (PANalytical, Netherlands); scanning electron microscope (SEM) images of synthetic materials were obtained by field emission scanning electron microscope JSM-7800F (JEOL, Japan). Electrochemical impedance spectroscopy was performed using an electrochemical workstation (ZAHNER, Germany) in 5 mM $[Fe(CN)_6]^{3-/4-}$, the solution containing 0.5 M KCl, scanning the frequency is 1 Hz - 1×10^4 Hz and 10 mV amplitude. Electrochemical measurements were performed using a CHI660E electrochemical workstation (Shanghai Chenhua, China) based on a three-electrode system including a modified GCE electrode as a working electrode, an Ag/AgCl electrode was used as a reference electrode (3 M KCl concentration), and a platinum wire was used as an auxiliary electrode. Cyclic voltammetry (CV) measurements had a potential window of − 0.6 to 0.1 V at 100 mV/s. For the chronoamperometry(it) measurement, the potential was selected to − 0.15 V.

Preparation of MXene-Au@Pt nanoflower material

Etching method: 1.6 g lithium fluoride was dissolved slowly in 20 mL 9 M hydrochloric acid with stirring for 5 min, then added 1 g Ti_3AlC_2 (for 10 min) slowly and stirred it for 24 h at room temperature. Then, deionized water was used to wash it and centrifuged about 6–8 times with a 3500 rpm speed for 5 min each time, so that the pH of the solution was larger than 6. The precipitate was collected and dissolved in 100 mL water, then sonicated for 3 h under the argon-protected atmosphere. At last, the supernatant was $Ti_3C_2T_X$ collected after centrifuging for 1 h with a speed of 3500 rpm. The resulting precipitate added with deionized water was sonicated in an ice bath for 1 h to delaminate the $Ti_3C_2T_X$ flakes. Finally, the obtained supernatant was collected after centrifuged at 8000 rpm for 1 h. The obtained supernatant was vacuum dried to obtain a black powder, a certain amount of $Ti_3C_2T_X$ was weighed into a 5 mM solution, and 3 mL chitosan (0.5%) was added to 30 mL Ti_3C_2Tx solution (0.5 M). H_2PtCl_6 (3 mM) solution and 2.5 mL $HAuCl_4$ (5 mM) and 2.5 mL of 0.1 M of ascorbic acid (AA) were stirred for 0.5 h to prepare MXene-Au@Pt nanoflower solution. The synthesis process is shown in Fig. 1.

Construction of Enzyme Biosensor Based on $Ti_3C_2T_X$-Au@Pt Nanoflowers

The construction of an enzyme biosensor based on $Ti_3C_2T_X$-Au@Pt nanoflowers was mainly prepared by a drop coating method. Before the electrode was constructed, the GC electrode was sequentially polished on a polishing cloth using 0.3 μm and 0.05 μm alumina powders, respectively, and was washed by ultrapure water, then was separately sonicated in alcohol and ultrapure water, and finally was blown dry with nitrogen. A multilayer film of GCE/$Ti_3C_2T_X$-Au@Pt nanoflowers/5′-nucleotidase-xanthine oxidase/bovine serum albumin (BSA) was prepared at 25 °C room temperature according to the following procedure. The 5 μL $Ti_3C_2T_X$-Au@Pt nanoflower solution was dropped onto the surface of the GCE and dried in the air. Then, 5 μL nucleotide oxidase-xanthine oxidase solution (5′-nucleotidase:xanthine oxidase = 1:1) was immobilized on the surface of GCE/$Ti_3C_2T_X$-Au@Pt nanoflowers and dried. Finally, 5 μL BSA (1%) solution was added dropwise and dried, and the obtained sensor was thoroughly washed with PBS and stored at 4 °w. The assembly process of the enzyme biosensor is shown in Fig. 2.

Preparation of Samples

Five-gram meat sample was homogenized with 20 mL 5% perchloric acid at 10,000 rpm for 3 min using a homogenizer (JRA-35S, China) and then diluted it to 25 mL with 5% perchloric acid. The homogenate was placed in a centrifuge (Allegra, USA) and centrifuged with a 15,000 rpm speed for 10 min at 4 °C, and supernatant was collected. The supernatant was adjusted to pH 5.5 with KOH, and then centrifuged at 15,000 rpm for 10 min at 4 °i, and the supernatant was collected for high-performance liquid chromatography analysis.

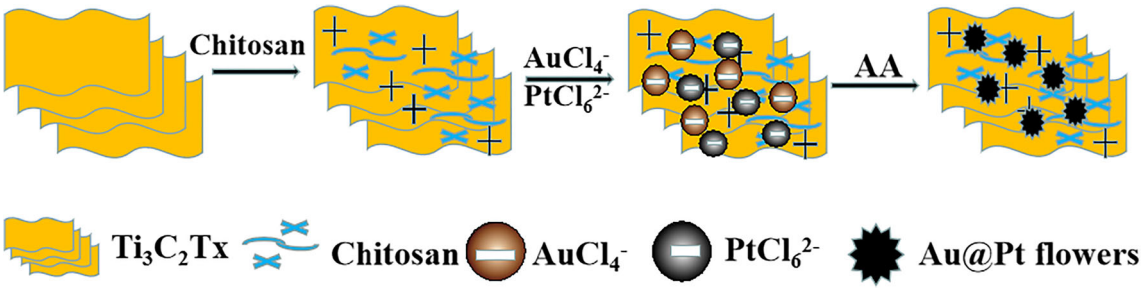

Fig. 1 Schematic illustration for the preparation of Au@Pt/GO nanocomposites

Comparative Analysis Results

The sample was chromatographed at 30 °h using a C18 column. Mobile phases A and B were phosphate buffer and 100% methanol. After 5-min isocratic run with 100% elution solvent A, the ratio of elution solvent B increased linearly from 3 to 10 min to 35%, from 10 to 15 min to 50%, and kept 10 min. Thereafter, the column was washed with 100% elution solvent B for 10 min. The column was equilibrated with 95% eluting solvent A for 30 min. Ten-microliter sample was filtered through a 0.45-μm PESU filter and then injected into the column at a flow rate. The detection wavelength was set at 254 nm per minute at 1.5 mL. The peak was detected at 254 nm with a Water 2998 PDA detector. Peaks were identified by comparing retention times with standards, and the concentration of IMP was determined by the peak area.

Results and Discussion

SEM and XRD Characterization of MXene

In this experiment, MXene-$Ti_3C_2T_X$ nanosheets were synthesized by stripping Al layers from the original Ti_3AlC_2 phase with a mixed solution of HF and HCl at room temperature (Zhang et al. 2017). The prepared MXene-$Ti_3C_2T_X$ nanosheets were characterized by SEM and XRD (Fig. 3).

It could be clearly seen from Fig. 3 (A) that the synthesized MXene-$Ti_3C_2T_X$ material exhibited graphene-like multilayer nanostructures and had its unique lamellar structure, which provided a large number of attachment sites for Au@Pt nanoflowers. At the same time, its 2D graphene-like nanostructures provided an ultra-large specific surface area for the immobilization of 5′-nucleotidase-xanthine oxidase, and the 5′-nucleotidase-xanthine oxidase which could be absorbed by the surface functional groups of MXene. As shown in Fig. 3 (B), MXene/Au@Pt nanoflower composite film was formed on the GCE electrode. The 2D nanolayer structure provided by MXene material was beneficial to retain the entrapped enzyme biological activity and promote the transport of enzymes and products. At the same time, MXene/Au@Pt nanoflower composite membrane had good electron transfer effect. With good catalytic properties, the enzymatic hydrolysate H_2O_2 could monitor the electrical signal changes in the enzymatic hydrolysis process in time, and could achieve qualitative and quantitative detection of IMP. MXene-$Ti_3C_2T_X$ was scanned in the 2θ range of 0–100° to identify the crystal structure. As shown in Fig. 3 (C), there were several very sharp diffraction peaks indicating the crystalline structure. The main diffraction characteristic peaks observed at 8.9°, 13.7°, and 27.5°, respectively, which were very consistent with the XRD spectrum of the previously reported MXene-Ti_3C_2Tx (Scheibe et al. 2019). It was indicated that crystalline material MXene-$Ti_3C_2T_X$ had a –OH surface ligand. During the etching process, the unsaturation of unpaired electrons was easily bonded by various functional groups (–O, –F, or –OH) (Sinha et al. 2018). Because MXene-$Ti_3C_2T_X$ material was prepared in water, the surface part of MXene-$Ti_3C_2T_X$ material was combined with –OH functional group, which made it good dispersibility in water. Since the surface of the material

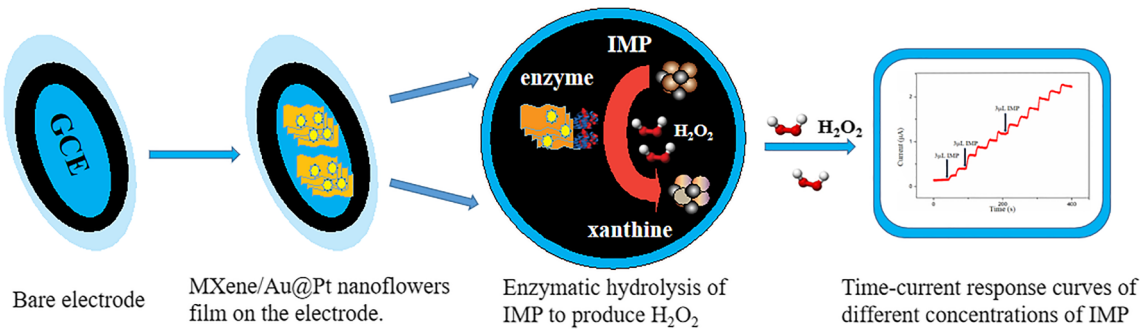

Fig. 2 GCE/$Ti_3C_2T_X$-Au@Pt nanoflowers/5′-nucleotidase-xanthine oxidase modification process

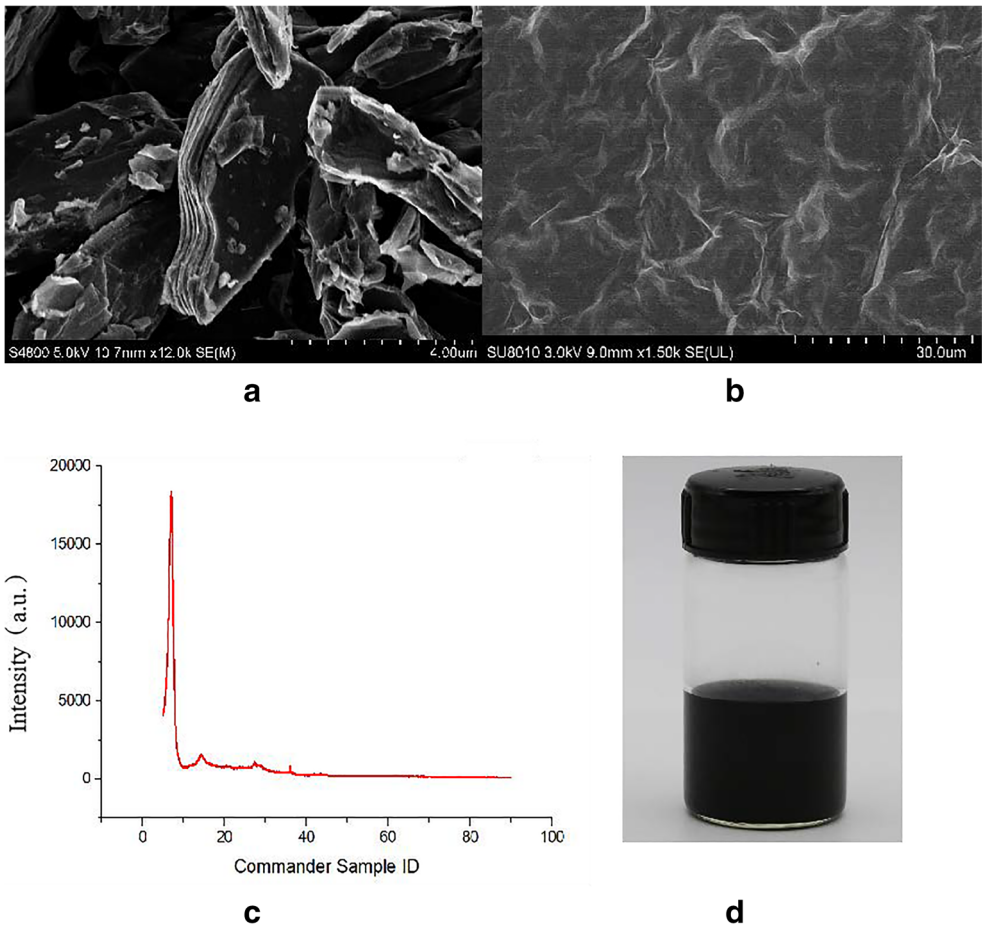

Fig. 3 (A) Typical SEM image of MXene. (B) SEM image of MXene/Au@Pt nanoflower film on the electrode. (C) XRD image of MXene. (D) Dispersion photograph of 0.5 mg mL^{-1} MXene-$Ti_3C_2T_X$ in an aqueous solution

was rich in hydroxyl groups, Fig. 3 (D) showed that MXene-$Ti_3C_2T_X$ was uniformly dispersed in the aqueous phase, which brought great convenience to the preparation of the enzyme biosensor and also changed the stability and reproducibility of the sensor.

Characterization of MXene/Au@Pt Nanoflower Composites

The morphology, composition, and structure of MXene/Au@Pt nanoflower composites were characterized by SEM, TEM, and EDS. As shown in Fig. 4 (A) and (B), the surface of the GCE electrode was modified with black MXene-$Ti_3C_2T_X$. The dandelion-like nanosphere was composed of Pt particles centered around the Au particles (Yang et al. 2018). Therefore, it may be the different reduction potentials of $AuCl^{4-}$/Au and $PtCl_6^{2-}$/Pt that caused the shell-core structure between the center and the shell (Shima et al. 2019). Figure 4 (C) and (D) showed the EDS spectra of MXene/Au@Pt nanoflowers, confirming the existence of C, Ti, Au, and Pt elements and demonstrating the successful synthesis of MXene/Au@Pt nanoflower conductive films.

Electrochemical Characterization of MXene/Au@Pt Nanoflower Modification Materials

The surface of the modified electrode was examined in a solution containing 5 mM $[Fe(CN)_6]^{3-/4-}$ and 0.1 M KCl. The stability of the modified MXene material compared with the modified Au@Pt-MXene material under the same conditions for 4 cycles is shown in Fig. 5 (A). The results showed that only the CV image of the electrode of MXene material was modified. As the number of scanning turns increasing, the redox peak gradually decreased. It was reported that $Ti_3C_2T_X$ would be gradually oxygenated to TiO_2 after energization (Peng et al. 2017). Based on the observation and the data published in the literature, oxidized $Ti_3C_2T_X$ meets the following formula during exposure to the anode potential:

$$Ti_3C_2Fx + 8H_2O = 3TiO_2 + 2CO + 16H^+ + (16\text{-}x)e\text{-} + xF^-$$

The conductivity of TiO_2 in the oxidation product was reduced relative to $Ti_3C_2T_X$. However, the stability of the MXene material with Au@Pt nanoflowers greatly enhanced and the redox peak was more obvious. The reduction peak appeared at 0.2 V, and the oxidation peak appeared at 0.27 V. It could be seen from Fig. 5 (B) that the oxidation peak of the MXene/Au@Pt nanoflower modified electrode was

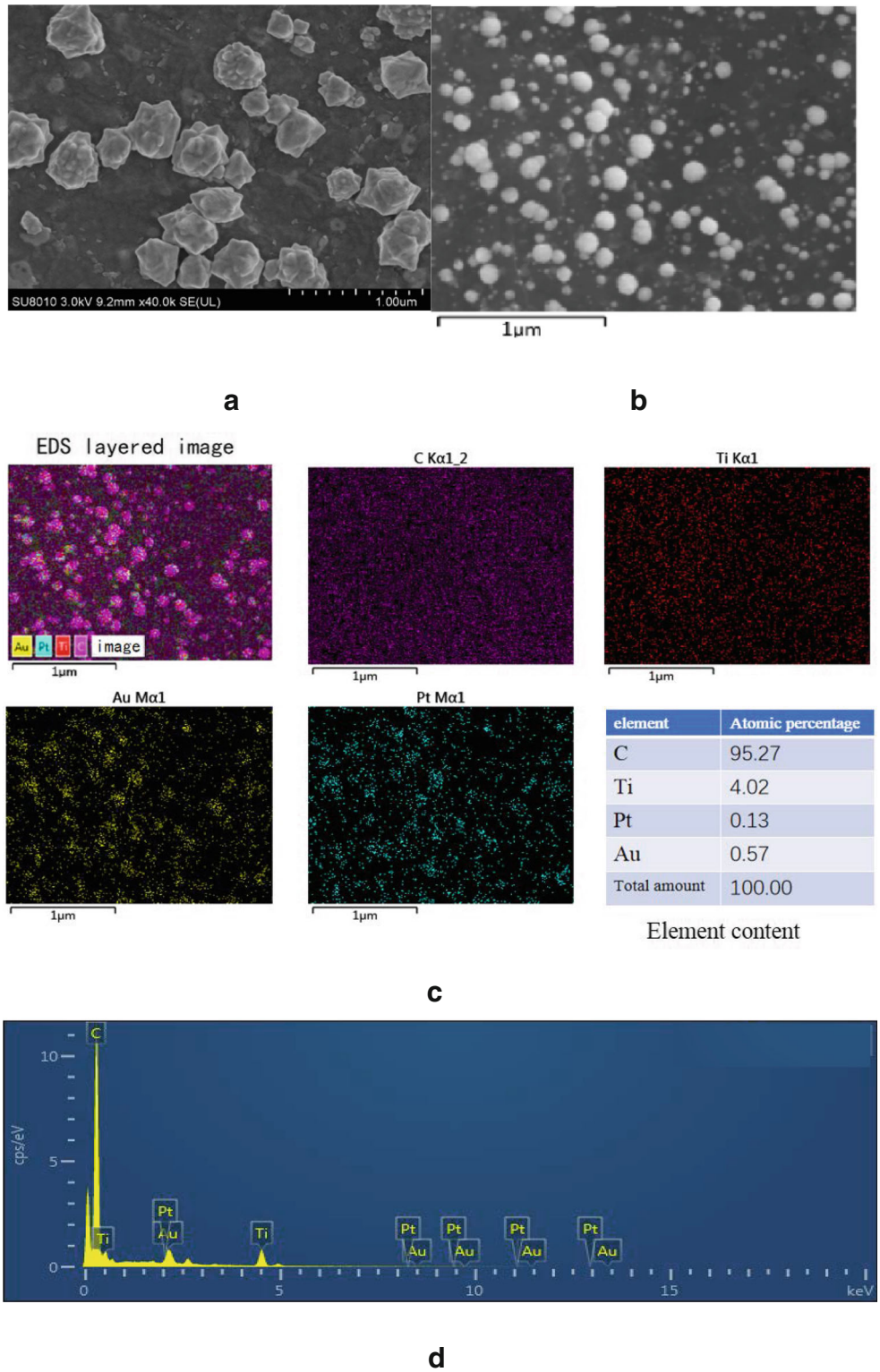

Fig. 4 (A) SEM image of MXene/Au@Pt nanoflower composite. (B) TEM image of MXene/Au@Pt nanoflower composite. (C) MXene/Au@Pt nanoflower composite EDS layered image. (D) MXene/Au@Pt nanoflower composite material spectrum image

basically the same after four cycles, and the steady state value of the MXene/Au@Pt nanoflower modified material was much higher than that of the original MXene material (85% of initial current). In the original case, the gradual decreasing of MXene conductivity was caused by the formation of TiO_2 nanoparticles and subsequent dissolution of MXene (Shahzad et al. 2018). This indicated the great stability of MXene/Au@Pt nanoflower modified material on anode potential window of various electrochemical sensing platforms. AC impedance (EIS) was a kind of technique for characterizing the

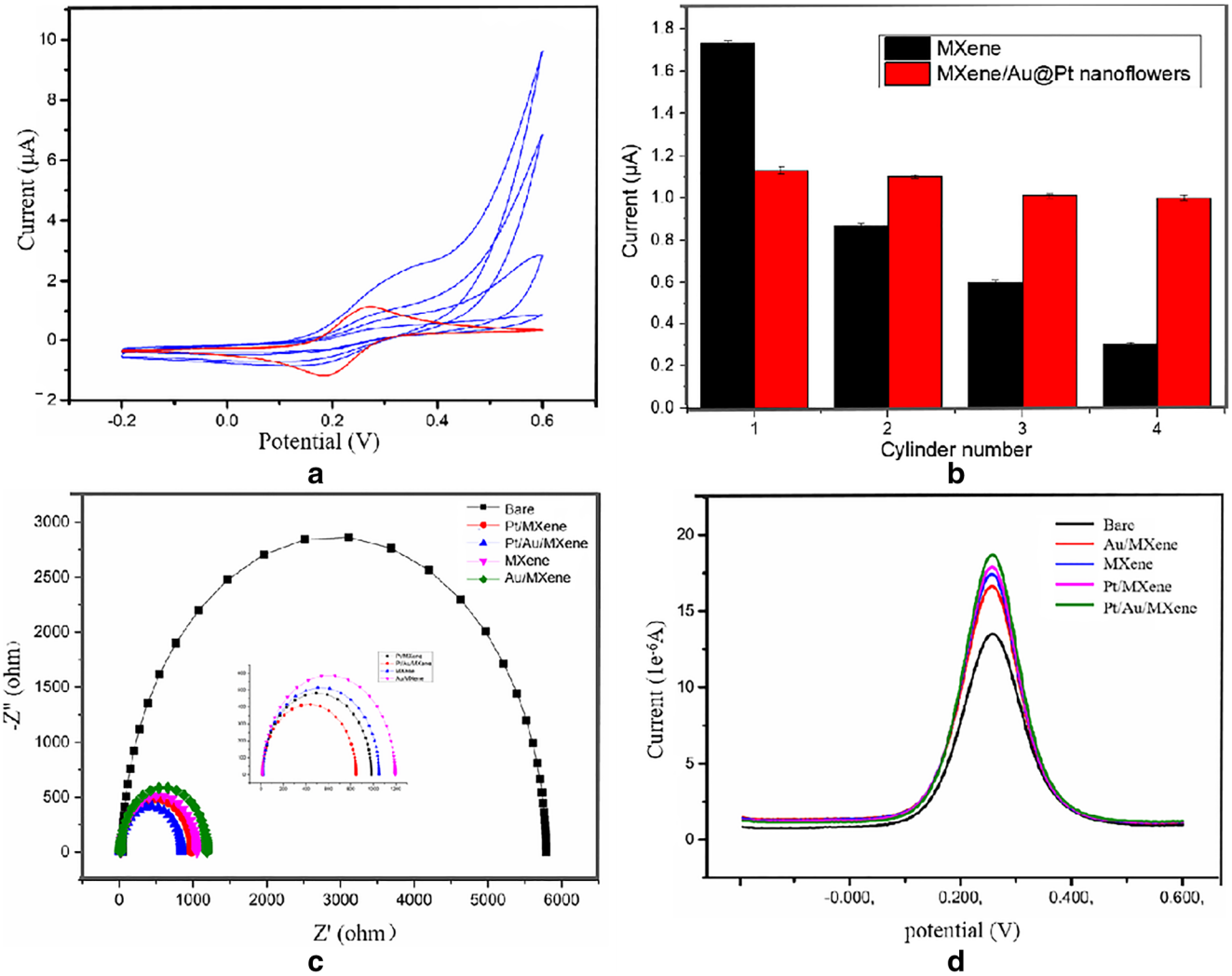

Fig. 5 (A) MXene/Au@Pt-MXene modified material CV cycle 4 lap image. (B) MXene/Au@Pt-MXene modified material CV oxidation peak data comparison column chart. (C) GCE/MXene/Au-MXene/Pt-MXene/Au@Pt-MXene modified material EIS map. (D) GCE/MXene/Au-MXene/Pt-MXene/Au@Pt-MXene modified material DPV chart

interfacial properties of nanocomposite-modified GCE electrodes. Figure 4 (C) showed the impedance spectra of GCE/MXene/Au-MXene/Pt-MXene/Au@Pt-MXene modified materials in solution which contained 5 mM $[Fe(CN)_6]^{3-/4-}$ and 0.1 M KCl. In the Nyquist diagram, the high-frequency semicircular portion corresponds to the electron transfer process and its diameter was equal to the electron transfer resistance (Rct) (Camacho et al. 2017). As shown in Fig. 5 (C), bare electrode resistance was the largest, indicating that the resistance of the bare electrode was up to 5.7 kΩ. When the MXene material was modified on the electrode, the diameter of the semicircle was significantly reduced to 1.1 kΩ, indicating that the MXene material had excellent conductivity. When modificated separately by Au particles and Pt particles and Au@Pt nanoflowers, the conductivity of MXene material was similar, which proved that modified Au@Pt nanoflowers cannot affect the conductivity of MXene and it also had good conductivity. At the same time, the corresponding modified electrode was detected by differential pulse voltammetry (DPV). As shown in Fig. 5 (D), the current peaks of the different modified materials at the 0.27-V point were different and the peak potential of the bare electrode was at $1.3e^{-5}$. With the difference of the modified materials, modified MXene-Au@Pt nanoflowers had the highest peak electrode current, reaching $1.8e^{-5}$, which verified the detection result in the Nyquist diagram. Based on the above characterization results, the electrode modified by MXene-Au@Pt nanoflowers had a good conductivity in $K_3[Fe_3(CN)_6]$ solution and could be used as a nanolevel electrode to promote electron transfer to the electrode surface.

Optimization of Experimental Parameters

The activity of the enzyme was affected by temperature, and the effect of temperature on the activity of the enzyme was studied (Matyushov 2018). The experiments were carried out

at 5 °C, 15 °C, 25 °C, 35 °C, 45 °C, and 55 °C respectively. As shown in Fig. S1, the peak current of the DPV was the highest when the temperature of the electrolyte was 35 °C. Thus, 35 °C was chosen as the optimum temperature in the following experiment.

The change of pH not only affected the activity of enzyme but also changed the conductivity of the material which modified electrode (Li et al. 2018a, b, c). Therefore, the effect of pH on biosensors was studied. DPV image of enzyme biosensor in inosine in solution with pH range of 3.0–9.0 was studied. It showed that the peak value of current increased with the increasing of pH value, as shown in Fig. S2. But the peak value drops when pH was 6.0, so pH 6.0 was selected as the optimum pH value of the electrolyte.

Different ratios of 5′-nucleotidase and xanthine oxidase also affected the electrochemical behavior of IMP, because xanthine oxidase would act on the product of 5′-nucleotidase. The DPV peak current of the sensor was observed based on 5′-nucleotidase in different proportions. In Fig. S3, the peak current was the highest when ratio of double enzyme was 1:1, so the 1:1 was chosen as the best ratio.

Electrochemical Characteristics of Biosensor Based on MXene

To verify the bioelectrochemical activity of the MXene-Au@Pt/5′-nucleotidase-xanthine oxidase/BSA biosensor, the prepared electrode was characterized by CV in the presence of IMP with a potential window ranging from − 0.6 to 0.6 V. Figure 6 (A) showed CV image obtained from various scanning rates of MXene-Au@Pt/5′-nucleotidase-xanthine oxidase/BSA biosensor in deoxygenated PBS buffer (0.01 M, pH 6.0). As shown in Fig. 6 (B), the cathode and anode peak currents increased linearly as the scan rate increasing, which indicated that electron transfer between the 5′-nucleotidase-xanthine oxidase and the GCE electrode can be carried out on the MXene-Au@Pt nanoflower composite membrane. According to the Laviron equation to carry out electrochemical characterization, the peak current was proportional to the scan rate and increased with scan rate increasing. And cathode and anode peak potentials were independent of scan rate (Laviron 1997).

In the presence of oxygen, IMP can be hydrolyzed by the relevant enzymes to hypoxanthine and hydrogen peroxide (Sun et al. 2016). Here, IMP performs qualitative and quantitative detection by changing the electrical signal generated by the oxidation of hydrogen peroxide with horseradish peroxidase. In this experiment, IMP was hydrolyzed to hypoxanthine and hydrogen peroxide by using nucleotidase, and in addition, hypoxanthine was further hydrolyzed to xanthine and hydrogen peroxide by xanthine oxidase. Au@Pt nanoflowers on the electrodes can catalyze the oxidation of hydrogen peroxide sensitively (Sanzò et al. 2017). Table 1 compares this work with the literature for H_2O_2 testing. By detecting changes in the electrical signal of hydrogen peroxide during the two-step enzymatic hydrolysis process, the detection limit of IMP is lower at 4.54 μA mM^{-1} cm^{-2} Figure 7 shows the presence and absence of a CV image of IMP (b). When 3 μM of IMP was injected, the oxidation current and the reduction current increased significantly. An increase in the redox current indicates that the enzyme catalyzed reaction occurs on the surface of the electrode, and the 5′-nucleotidase/xanthine oxidase immobilized on the electrode is highly biocatalytic to IMP.

Differential pulse voltammetry (DPV) applied a step potential to the electrode, which was more sensitive and had a higher resolution ratio than CV image. It had a good detection capability, with detection concentration as low as 1 μe L^{-1}

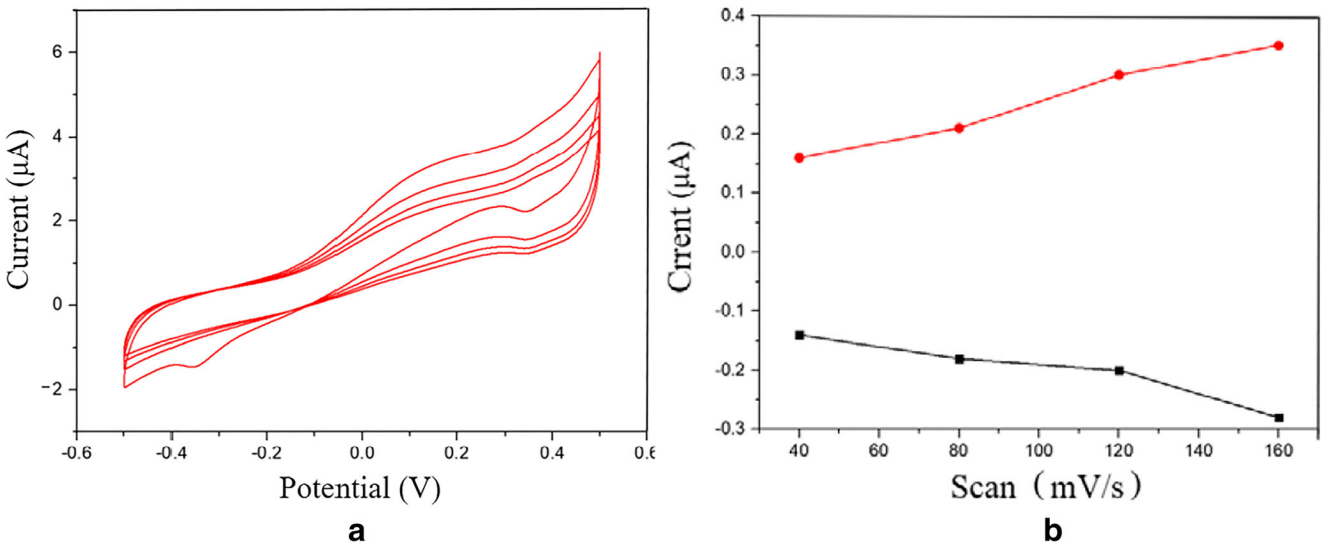

Fig. 6 (A) CV curve of MXene-Au@Pt/5′-nucleotidase-xanthine oxidase/BSA biosensor in PH = 6.0 PBS with different scanning rates (from inside to outside: 40, 80, 120, 160 mV/s). (B) Cathode and anode peak current versus scan rate calibration curves

Table 1 Comparison between this work and the literature regarding H_2O_2 detection

Sensor	Sensitivity μAmM^{-1} cm^{-2}	Linear range μM	LOD μM	Refs
GF/Co_3O_4-NPs/GCE	1.14	0.2–211.5	0.06	(Karuppiah et al. 2014)
MNPs@MOFs/ERGO	-	4–1.1 × 10^4	0.18	(Li et al. 2018a, b, c)
Cu_2O-rGO_{pa}	20.07	30–12,800	21.7	(Xu et al. 2013)
Cat/AuNPs/graphene-NH2/GCE	13.4	0.3–600	0.05	(Huang et al. 2011)
Au–Pd–Pt/MoS_2	-	0.001–0.1	0.0003	(Dou et al. 2018)
RGO/ZnO/GCE	13.49	0.02–22.48	0.02	(Palanisamy et al. 2012)
Au/rGO	1238.00	0.02–10.00	0.10	(Dhara et al. 2016)
Fe_3O_4 nanodots	-	2.5–6.5 × 10^3	1.1	(Bas et al. 2018)
GRO/Pt-AgNPs/GCE	699.6	5–1500	0.04	(Zhang et al. 2016)
PDDA/ERGO-ATP-Pd/GCE	492.09	0.1–1000	0.016	(You et al. 2013)
Mxene-Ti_3C_2Tx/Pt@Au/GCE	4.54	0.5–1200	0.00085	This work

(Chng et al. 2014). Figure 8 (A) showed the DPV (b) curve with the addition of IMP had a higher current peak compared with the DPV (a) curve without the addition of IMP. The current peak was around − 0.15 V, indicating that maximum response current of enzyme biosensor to IMP can be observed near the relatively low potential of − 0.15 V. In order to reduce the background interference factor effectively and have a lower detection limit, − 0.15 V was used as a fixed voltage for further amperometric electrochemical characterization. Compared with the CV method, amperometric method was an electrochemical method that was more sensitive to the detection of IMP. Figure 8 (B) showed the time-current curve of the MXene-Au@Pt/5′-nucleotidase-xanthine oxidase/BSA biosensor at a fixed potential of − 0.15 V in PBS (50 mM); the test was carried out under constant agitation in the buffer. The MXene-Au@Pt/5′-nucleotidase-xanthine oxidase/BSA biosensor was used to detect IMP, and a gradient curve was showed when 3 μL IMP (3 μM) was added every 30 s, indicating 5′-nucleotidase/xanthine oxidase was immobilized on the electrode and still retained biocatalytic activity. The response time of the electrode modified by MXene-Au@Pt/5′-nucleotidase/xanthine oxidase/BSA was less than 5 s (98% of steady state current was reached). The rapid response of MXene-Au@Pt/5′-nucleotidase/xanthine oxidase/BSA biosensor could be attributed to the diffusion of IMP from the external solution to the 5′-nucleotidase/xanthine oxidase immobilized on the MXene nanosheets and its rapid biocatalytic reaction, which could produce hydrogen peroxide. The gradient current curve was generated via the change of current signal generated by the rapid catalytic oxidation of hydrogen peroxide. A typical calibration curve for the response current of the enzyme biosensor and IMP concentration is shown in Fig. 8 (C). As the concentration of IMP increasing, the current increased. Based on the MXene-Au@Pt/5′-nucleotidase/xanthine oxidase/BSA biosensor, the linear range was from 0.2 to 210 ng mL^{-1}, and it showed a good linear relationship with a correlation coefficient of 0.9964. The detection limit (LOD) of MXene-Au@Pt/5′-nucleotidase/xanthine oxidase/BSA biosensor was 0.224 ng mL^{-1}, which was superior to the enzyme biosensor constructed by polypyrrole-Au (Dervisevic et al. 2017). MXene-Au@Pt/5′-nucleotidase/xanthine oxidase/BSA biosensor with low LOD and wide linear range had a great biosensor performance which was attributed to the following aspects: firstly, MXene had a 2D lamellar structure similar to graphene, provided abundant binding sites for Au@Pt nanoflowers, and increased the loading of nanoflowers. In addition, it also had good electrical conductivity, providing favorable conditions for the transmission of electrons and amplifying electrical signal. That made it more sensitive. At the same time, its good biocompatibility provided a favorable microenvironment for the immobilization of related enzymes to maintain their activity and stability. The

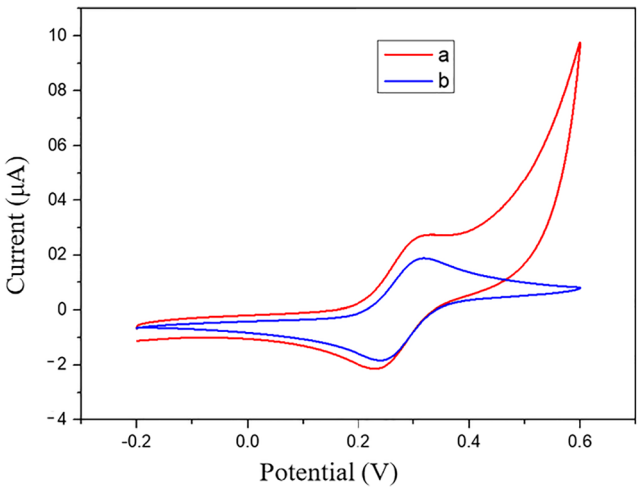

Fig. 7 MXene-Au@Pt/5′-nucleotidase-xanthine oxidase/BSA biosensor in the presence of 3 μM IMP (a) and in the absence of IMP (b) at 50 mM PH 6.0 CV plot at a scan rate of 100 mV/s in PBS buffer

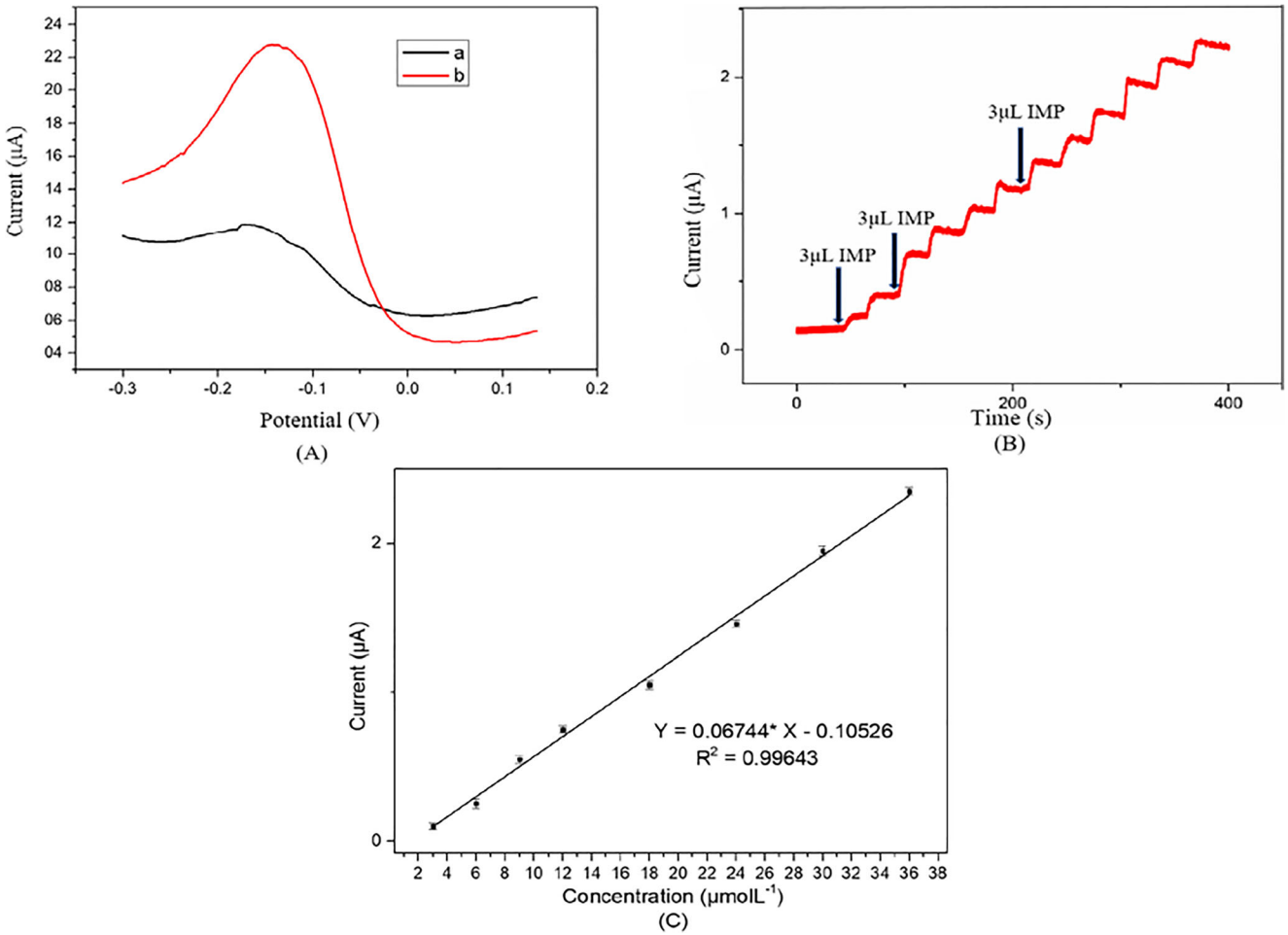

Fig. 8 (A) MXene-Au@Pt/5′-nucleotidase-xanthine oxidase/BSA biosensor in the presence of 3 μM IMP (a) and in the absence of IMP (b) scanning DPV. (B) Time-current response curves of different concentrations of IMP at MXene-Au@Pt/5′-nucleotidase-xanthine oxidase/BSA biosensor at a potential of − 0.15 V. All tests were detected at a rate of 100 mV/s in 50 mM PH 6.0 PBS buffer agitation. (C) Corresponding calibration curve for steady state current versus inosine concentration

MXene-Au@Pt biosensor could be a promising and powerful biosensing platform for hypersensitivity and rapid detection of IMP.

Performance of Biosensor

Studies have shown that IMP is associated with purines and pyrimidines, especially inosine diphosphates and inosine triphosphates, which can be considered possible interfering compounds (Matsumoto et al. 1998; Bakshi et al. 2006). As shown in Fig. 9, when the IMP was added to the PBS buffer, the current signal became larger, indicating that there was a catalytic reaction. However, there was no current response when the interference was added, indicating that the sensor had a good specificity and anti-interference. The stability of the constructed biosensor was further tested by square wave voltammetry (SWV). The standard deviation of MXene-Au@Pt/5′-nucleotidase/xanthine oxidase/BSA biosensor was 3.4% after continuous measurement (10 times), which showed

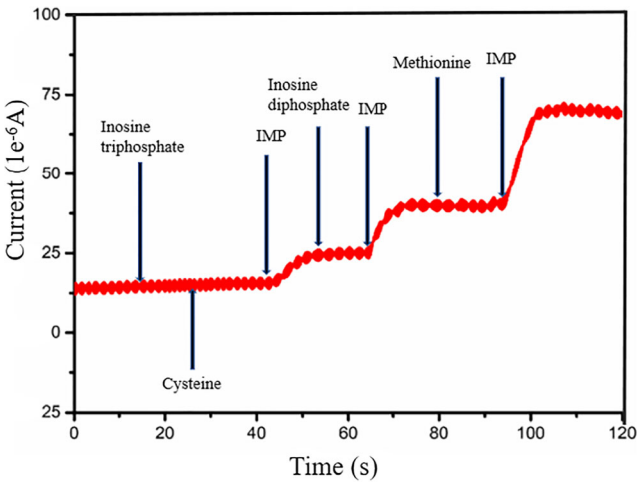

Fig. 9 Adding inosine triphosphate (1 g L^{-1}), cysteine (1 g L^{-1}), inosine diphosphate (1 g L^{-1}), methionine (1 g L^{-1}), inosine (0.1 g L^{-1}). The ampere response of the sensor in PBS buffer was constant at − 0.15 V

Table 2 Comparison of IMP content in actual samples by two methods

Sample	Chicken	Pork	Beef	Lamb
LC (mg/g)	1.88 ± 0.17	0.97 ± 0.21	2.44 ± 0.15	1.17 ± 0.19
Biosensor (mg/g)	1.86 ± 0.07	0.94 ± 0.06	2.40 ± 0.05	1.07 ± 0.09
Relative deviation	− 1%	− 3%	− 1.6%	− 8.5%

great stability. In addition, the sensor was stored in a 4 °C refrigerator for 2 weeks and the response remained at 95% of its original activity. The results showed that the reproducibility of the biosensor was satisfactory.

Application of Biosensor

In order to further demonstrate the utility of the constructed sensor, four different meat samples were analyzed via the constructed biosensor, including chicken, pork, beef, and lamb. LC was used as a reference method (Table 2). Compared with the electrochemical detection results of LC detection, the partial error data is basically the same, the error comes from the same sample time difference, and the error is within a reasonable range, indicating that the constructed biosensor can be effectively applied to the actual sample.

Conclusions

In this paper, MXene-Au@Pt nanoflower composites with conductivity and biocompatibility were prepared by one-step synthesis. The MXene-Au@Pt/5′-nucleotidase/xanthine oxidase/BSA double-enzyme biosensor was prepared for the detection of IMP in fresh meat. The qualitative and quantitative detection of IMP is achieved by the by-product H_2O_2 produced after enzymatic hydrolysis. The sensor uses dual enzymes to quantitatively detect IMP in fresh meat. The double-enzyme biosensor has good catalytic activity for IMP. The H_2O_2 further increased in the enzymatic hydrolysis process to increase the detection signal. The core-shell nanoflowers formed by Au@Pt can effectively catalyze the by-product H_2O_2 produced by oxidation, without being disturbed by environmental conditions. The MXene-Au@Pt nanoflower enzyme biosensor has the advantages of wide linear range, high sensitivity, and rapid detection of IMP. The sensor with good application prospects was prepared for the method proposed in this paper, which can be used for meat quality evaluation.

Funding Information This work was supported by the National Natural Science Foundation of China (No. 31772068, 31701681, 31872909), Special Project of Independent Innovation of Shandong Province (2018CXGC0214), Shandong Provincial Natural Science Foundation (ZR2017BC001, ZR2018ZC0126, ZR2018BC055).

Compliance with Ethical Standards

Ethical Approval This article does not contain any studies with human participants performed by any of the authors.

Informed Consent Not applicable.

Conflict of Interest Guangxian Wang declares that there is no conflict of interest. Jianfei Sun declares that there is no conflict of interest. Yao Yao declares that there is no conflict of interest. Xingshuang An declares that there is no conflict of interest. Hui Zhang declares that there is no conflict of interest. Guanglei Chu declares that there is no conflict of interest. Shui Jiang declares that there is no conflict of interest. Yemin Guo declares that there is no conflict of interest. Xia Sun declares that there is no conflict of interest. Yuan Liu declares that there is no conflict of interest.

Novelty Statement A novel enzyme biosensor was developed to assess meat quality and freshness. Using the conductivity of MXene materials and the catalytic activity of Au@Pt nanoflowers, the enzyme biosensor was assembled and prepared for ultra-sensitive and rapid detection of IMP. The MXene-$Ti_3C_2T_X$ material had a 2D nanostructure similar to graphene, as well as metal conductivity and good biocompatibility. Used as a carrier for related enzymes, MXene provided a good biological environment and a stable microenvironment, while the bimetallic nanoflowers with a core-shell structure had higher catalytic activity than a single noble metal. The by-product hydrogen peroxide was produced by the double-enzyme catalysis process used, the current signal of the catalytic oxidation of hydrogen peroxide by Au@Pt nanoflowers was monitored at the biosensor as the detection target, and the qualitative and quantitative detection of IMP was achieved.

References

Bakshi MS, Kaura A, Bhandari P, Kaur G, Torigoe K, Esumi K (2006) Synthesis of colloidal gold nanoparticles of different morphologies in the presence of triblock polymer micelles. J Nanosci Nanotechnol 6(5):405–1410

Bas SZ, Cummins C, Borah D, Ozmen M, Morris MA (2018) Electrochemical sensing of hydrogen peroxide using block copolymer templated iron oxide nanopatterns. Anal. Chem 90(2):1122–1128

Camacho BR, Baltazar Vera JC, Ramı´rez AM, Ramı´rez RF, Aguilera GC (2017) EIS analysis of oxygen reduction reaction of Pt supported on different substrates. Int J Hydrogen Energy 42(51):30364–30373

Chekem CT, Goetz V, Richardson Y, Plantard G, Blin J (2019) Modelling of adsorption/photodegradation phenomena on AC-TiO_2 composite catalysts for water treatment detoxification. Catal Today 328(15): 183–188

Chng CE, Pumera M, Bonanni A (2014) Electrochemically reduced graphene nanoribbons: interference from inherent electrochemistry of the material in DPV studies. Electrochem Commun 46:137–139

Clausena MP, Christensena M, Djurhuusa TH, Duelunda L, Mouritsenb OG (2018) The quest for umami: Can sous vide contribute? Int J Gastron Food Sci 13:129–133

Dervisevic M, Dervisevic E, Evik EC, Senel M (2017) Novel electrochemical xanthine biosensor based on chitosanepolypyrroleegold nanoparticles hybrid bio-nanocomposite platform. J Food Druganal 25(3):510–519

Dhara K, Ramachandran T, Nair BG, Babu TGS (2016) Au nanoparticles decorated reduced graphene oxide for the fabrication of disposable

nonenzymatic hydrogen peroxide sensor. J. Electroanal. Chem 764: 64–70

Dou B, Yang J, Yuan R, Xiang Y (2018) Trimetallic hybrid nanoflower-decorated MoS_2 nanosheet sensor for direct in situ monitoring of H_2O_2 secreted from live cancer cell. Anal. Chem 90(9):5945–5950

Feng A, Yu Y, Wang Y, Jiang F, Yu Y, Mi L, Song L (2017) Two-dimensional MXene Ti_3C_2 produced by exfoliation of Ti_3AlC_2. Road Mater Pavement 114:161–166

Guo J, Zhao Y, Liu A, Ma T (2019) Electrostatic self-assembly of 2D delaminated MXene (Ti_3C_2) onto Ni foam with superior electrochemical performance for supercapacitor. Electrochim Acta 305: 164–174

Huang K, Niu D, Liu X, Wu Z, Fan Y, Chang Y, Wu Y (2011) Direct electrochemistry of catalase at amine-functionalized graphene/gold nanoparticles composite film for hydrogen peroxide sensor. Electrochimical Acta. 56(7):2947–2953

Karuppiah C, Palanisamy S, Chen SM, Veeramani V, Periakaruppan (2014) Novel enzymatic glucose biosensor and sensitive non-enzymatic hydrogen peroxide sensor based on graphene and cobalt oxide nanoparticles composite modified glassy carbon electrode. Sensor Actuat B-chem 196:450–456

Laviron E (1997) The use of polarography and cyclic voltammetry for the study of redox systems with adsorption of the reactants Heterogeneous vs surface path. Electroanal Chem 382(2):111–127

Li Z, Wang L, Sun D, Zhang Y, Liu B, Hu Q, Zhou A (2015) Synthesis and thermal stability of two-dimensional carbide MXene Ti_3C_2. Mat Sci End B-solid 191:33–40

Li B, Zhang D, Liu Y, Yu Y, Li S, Yang S (2017) Flexible Ti_3C_2 MXene-lithium film with lamellar structure for ultrastable metallic lithium anodes. Nano Energ 39:654–661

Li C, Wu R, Zou J, Zhang T, Zhang S, Zhang Z, Hu X, Yan Y, Ling (2018a) MNPs@anionic MOFs/ERGO with the size selectivity for the electrochemical determination of H_2O_2 released from living cells. Biosens Bioelectron 116:81–88

Li Q, Loman AA, Callow NV, Mahfuzul Islam SM, Ju LK (2018b) Leveraging pH profiles to direct enzyme production (cellulase, xylanase, polygalacturonase, pectinase, -galactosidase, and invertase) by Aspergillus foetidus. Biochem Eng J 137:247–254

Li Y, Deng X, Tian J, Liang Z, Cui H (2018c) Ti_3C_2 MXene-derived Ti_3C_2/TiO_2 nanoflowers for noble-metal-free photocatalytic overall water splitting. Applied Mater Today 13:217–227

Lorencova LK, Bertok T, Dosekova EK, Holazova A, Paprckova D, Vikartovska AC, Sasinkova V, Filip JL, Kasak P, Jerigova MK, Velic DS, Mahmoud KA, Tkac J (2017) Electrochemical performance of Ti_3C_2Tx MXene in aqueous media:towards ultrasensitive H_2O_2 sensing. Electrochim Acta 235:471–479

Lorencova LK, Bertok T, Filip J, Jerigova M, Velic D, Kasak P, Mahmoud KA, Tkac J (2018) Highly stable Ti_3C_2Tx (MXene)/Pt nanoparticles-modified glassycarbon electrode for H_2O_2 and small molecules sensing applications. Sensor Actuat B-chem 263:360–368

Matsumoto K, Asada W, Murai R (1998) Simultaneous biosensing of inosine monophosphate and glutamate by use of immobilized enzyme reactors. Anal Chim Acta 358:127–136

Matyushov DV (2018) Fluctuation relations, effective temperature, and ageing of enzymes: the case of protein electron transfer. J Mol Liq 266:361–372

Ngapo T, Vachon L (2016) Umami and related components in “chilled” pork for the Japanese market. Meat Sci 121:365–374

Palanisamy S, Chen SM, Sarawathi R (2012) A novel nonenzymatic hydrogen peroxide sensor based on reduced graphene oxide/ZnO composite modified electrode. Sens. Actuat. B 166-167:372–377

Peng C, Wang YH, Peng F (2017) TiO2-x/Ti3C2: synergy of active facets, interfacial charge transfer and Ti3+ doping for enhance photocatalytic activity. Meter Res Bull 89:16–25

Ramalingam VD, Song Z, Hwang I (2019) The potential role of secondary metabolites in modulating the flavor and taste of the meat. Food Res Int 122:174–182

Sanzò G, Taurino I, Puppo F, Antiochia R, Gorton L, Favero G, Mazzei F, Carrara S, Micheli GD (2017) A bimetallic nanocoral Au decorated with Pt nanoflowers (bio)sensor for H_2O detection at low potential. Methods 129:89–95

Scheibe B, Tadyszak K, Jarek M, Michalaka N, Kempiński M, Lewandowski M, Peplińska B, Chybczyńska K (2019) Study on the magnetic properties of differently functionalized multilayered Ti_3C_2Tx MXenes and Ti-Al-C carbides. Appl Surf Sci 479:216–224

Shahzad A, Rasoolb K, Nawaz M, Miran W, Jang J, Moztahida M, Mahmoud KA, Lee DS (2018) Heterostructural TiO_2/Ti_3C_2Tx (MXene) for photocatalytic degradation of antiepileptic drug carbamazepine. Chem Eng J 349:748–755

Shima K, Leeb WC, Parkc MS, Shahabuddind M, Yamauchie Y, Hossaina MA, Shimb YB, Kima JH (2019) Au decorated core-shell structured Au@Pt for the glucose oxidation reaction. Sensor Actuat B-Chem 278:88–96

Shukla VK, Jena NK, Naqvi SR, Luo W, Ahuja RJ (2019) Modelling high-performing batteries with Mxenes: the case of Sfunctionalized two-dimensional nitride Mxene electrode. Nano Energy 58:877–885

Sinha A, Dhanjai ZH, Huang Y, Lu X, Chen J, Jain R (2018) MXene: a emerging material for sensing and biosensing. Trac-trends AnalChem 105:424–435

Su X, Zhang J, Mu H, Zhao J, Wang Z, Zhao Z, Han C, Ye Z (2018) Effects of etching temperature and ball milling on the preparation and capacitance of Ti_3C_2 MXene. Jalloy Compd 752:32–39

Sun C, Gao L, Wang D, Zhang M, Liu Y, Geng Z, Xu W, Liu F, Bian H (2016) Biocompatible polypyrrole-block copolymer-gold nanoparticles platform for determination of inosine monophosphate with bi-enzyme biosensor. Sensor Actuat B-chem 230:521–527

Tran DT, Kshetri TL, Nguyen DC, Gautam JD, Hoa VH, Le HT, Kim NH, Lee JH (2018) Emerging core-shell nanostructured catalysts of transition metal encapsulated by two-dimensional carbon materials for electrochemical applications. Nano Today 22:100–131

Wang F, Yang CH, Duan M, Tang Y, Zhu J (2015) TiO_2 nanoparticle modified organ-like Ti_3C_2 MXene nanocomposite encapsulating hemoglobin for a mediator-free biosensor with excellent performances. Biosensors Bioelectronics 74:1022–1028

Wu W, Wei D, Zhu J, Niu D, Wang F, Wang L, Yang L, Yang P, Wang C (2019) Enhanced electrochemical performances of organ-like Ti_3C_2 MXenes/polypyrrole composites as supercapacitors electrode materials. Ceram Int 45:7328–7337

Xu F, Deng M, Li G, Chen S, Wang L (2013) Electrochemical behavior of cuprous oxideereduced graphene oxide nanocomposites and their application in nonenzymatic hydrogen peroxide sensing. Electrochimica Acta 88:59–65

Xu Z, Sun Y, Zhuang Y, Jing W, Ye H, Cui Z (2018) Assembly of 2D MXene nanosheets and TiO_2 nanoparticles for fabricating mesoporous TiO_2-MXene membranes. J Membrane Sci 564:35–43

Yang Z, Liu X, Zheng X, Zheng J (2018) Synthesis of Au@Pt nanoflowers supported on graphene oxide for enhanced electrochemical sensing of dopamine. J Electroanal Chem 817:48–54

You JM, Kim D, Kim SK, Kim MS, Han HS, Jeon S (2013) Novel determination of hydrogen peroxide by electrochemically reduced graphene oxide grafted with amino thiophenolePd nanoparticles. Sensor. Actuator. B 178:450–457

Zhang C, Zhang Y, Du X, Chen Y, Dong W, Han B, Chen Q (2016) Facile fabrication of Pt-Ag bimetallic nanoparticles decorated reduced graphene oxide for highly sensitive non-enzymatic hydrogen peroxide sensing. Talanta 159:280–286

Zhang T, Pan L, Tang H, Du F, Guo Y, Qiu T, Yang J (2017) Synthesis of two-dimensional Ti_3C_2Tx MXene using HClþLiF etchant:

Enhanced exfoliation and delamination. J Alloy Compd 695:818–826

Zhang H, Wang Z, Zhang Q, Wang F, Liu Y (2019a) Ti_3C_2 MXenes nanosheet catalyzed highly efficient electrogenerated chemiluminescence biosensor for the detection of exosomes. Biosensors Bioelectronics 124:184–190

Zhang J, Sun-Waterhouse D, Su G, Zhao M (2019b) New insight into umami receptor, umami/umami-enhancing peptides and their derivatives: a review. Trends Food Sci Tech 88:429or, u

Zhou L, Zhang X, Ma L, Gao J, Jiang Y (2017) Acetylcholinesterase/chitosan-transition metal carbides nanocomposites-based biosensor for the organophosphate pesticides detection. Biochem Eng J 128: 243–249